Econ. Environ. Geol.
Vol. 27, No. 2, p. 147-160, 1994.

The Geochemistry of Copper-bearing Hydrothermal Vein Deposits in Goseong Mining District (Samsan Area), Gyeongsang Basin, Korea

Sang Hoon Choi*, Chil Sup So*, Soon Hag Kweon* and Kwang Jun Choi*

ABSTRACT: Copper-bearing hydrothermal vein mineralization of the Samsan area was deposited in two stages (I and II) of quartz-calcite-sulfide veins which fill fissures in Cretaceous volcanic and sedimentary rocks of the Gyeongsang basin. The major ore minerals, chalcopyrite and sphalerite, together with pyrite, galena, hematite, and minor sulfosalts, occur with epidote and chlorite as gangue minerals in stage I quartz veins. Chlorite geothermometry, fluid inclusion and stable isotope data indicate that copper ore was deposited mainly at temperatures between 330℃ and 280℃ from fluids with salinities between 12 and 3 equiv. wt. % NaCl. Evidence of fluid boiling indicates a range of pressures from ≤100 to 200 bars.

Within ore stage I there was an apparent decrease in $\delta^{34}S$ values of H_2S with paragenetic time, from 8.0 to 2.3 per mil. This pattern was likely achieved through progressive increases in activity of oxygen accompanying boiling and mixing. In the early part of the first stage, the high temperature, high salinity fluids gave way to progressively cooler and more dilute fluids of the late parts in the first stage and of the second stage. There is a systematic decrease in calculated $\delta^{18}O_{water}$ values with decreasing temperature in the Samsan hydrothermal system, from values of −86 per mil for early portion of stage I through −5.9 per mil for late portion of stage I to −6.3 per mil for stage II. The δD values of fluid inclusion waters also decrease with paragenetic time from −76 per mil to −86 per mil. These trends combined with mineral paragenesis and fluid inclusion data are interpreted to indicate progressive cooler, more oxidizing meteoric water inundation of an early exchanged meteoric hydrothermal system.

INTRODUCTION

Most of copper bearing hydrothermal vein-type deposits occur within Cretaceous sedimentary, volcanic and igneous rocks in the Gyeongsang basin of the southeast of the Korean peninsula. These Korean Cu deposits provide an opportunity to investigate the influence of depth of granite emplacement on the post-magmatic evolution of hydrothermal systems, because the Cretaceous granites have been shown to have been emplaced to more shallow (<2~3 km, Reedman et al., 1975) levels than the Jurassic granites (>5 km).

In the past ten years there have been a number of geological studies of Cu-bearing deposits in the Gyeongsang basin; Sillitoe (1980), Min et al. (1982), Jin et al. (1982), Park et al. (1983), and Park et al. (1985).

The Cu-bearing hydrothermal veins in the Samsan area are entirely enclosed by the sedimentary rocks of Goseong formation and the tuffaceous and andesitic rocks of Upper Cretaceous Yucheon Group. The Jinheung, Samsan and Daedun mines are each located along such veins. The vein ores comprise mainly copper, lead, zinc and silver minerals. Average ore grade at Jinheung is about 8.18 wt. % Cu, 546 gram per metric ton Ag, and 2.3 gram per metric ton Au, these reserves are estimated about 345,088 metric tons. Samsan Cu mine is composed of at least three subparallel quartz veins. Its average ore grade is about 2.23 wt. % Cu and 194 gram per metric ton Ag. Ore reserves at Samsan are estimated about 45, 500 metric tons.

This paper documents the physico-chemical conditions of Cu mineralization, and the nature and evolution of the ore-forming fluids in the Samsan hydrothermal system.

GEOLOGY

Rocks of the Gyeongsang basin belong dominantly to the Gyeongsang Supergroup which consists mainly of a mixed sequence of postorogenic molasse-type sedimentary rocks intercalated with lavas and volcaniclastic rocks.

* Department of Geology, Korea University, Seoul 136-701, Korea.

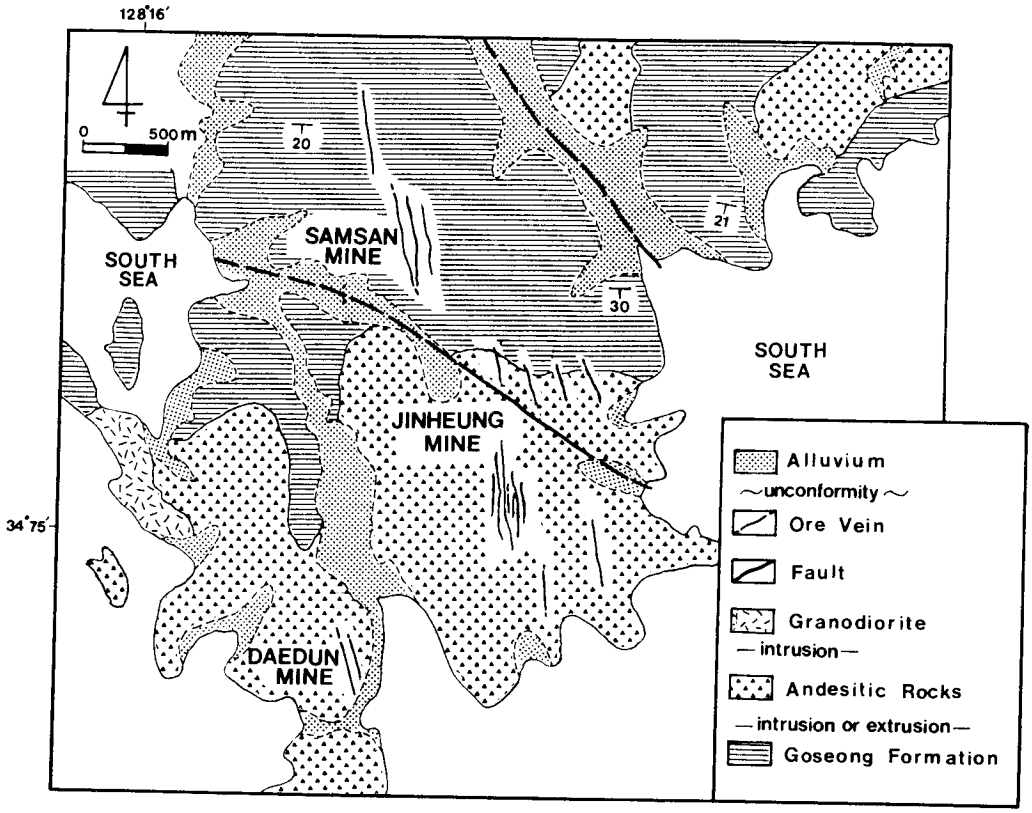

Fig. 1. Geologic map of the Samsan area.

Four main units of the Yucheon Group are found in the area (Fig. 1). They are, in ascending stratigraphic order: sedimentary rocks of Goseong Formation, andesitic lapilli-tuff, andesite sheets and welded tuff. The Goseong Formation consists of, in ascending order, a volcaniclastic conglomerate, a volcaniclastic sandstone, and a reddish volcaniclastic shale within which thin beds of greenish tuff are locally interbedded. In the area, the gray tuffaceous sandstone and the reddish tuffaceous shale occur as the lowermost and uppermost unit, respectively. The volcaniclastic sandstone is generally composed of rounded to subrounded grains of quartz, feldspar and andesite rock fragments embedded in a groundmass of fine-grained muscovite, calcite, and iron oxides. The volcaniclastic shale occurs as thin beds (≈10 cm thick) and consists of angular grains of quartz, feldspar, muscovite, and andesite rock fragments, and a matrix of iron oxides. The andesitic lapilli-tuff is composed of an andesitic matrix with fragments of aphanitic andesite and tuff, plagioclase grains, and small amounts of epidote, calcite, and iron oxides. The andesites occur as both intrusive and extrusive rocks and commonly intrude the andesitic lapilli-tuff.

Fine to medium-grained granodiorite of the 'Cretaceous Bulgugsa Series' intrude the previously described sedimentary and volcanic rocks. These plutonic rocks are confined generally to the southeastern portion of the Korean peninsula and are associated with many of Korean epigenetic ore deposits (Lee, 1981).

DATING OF IGNEOUS ACTIVITY AND MINERALIZATION

A date was obtained for alteration adjacent to the mineralized vein in the Goseong district using K-Ar dating method (Table 1). A small granodiorite stock occurs west of the mining area. The granodiorite yielded an Rb-Sr date of 105± 5 Ma (So et al., 1985). Shelton et al. (1990) show that the granodiorite in the Tongyoung Au-Ag mine area yielded a two point Rb-Sr isochron date of 105.0± 5.0 Ma (Table 1), indicating a Cretaceous age of emplacement. Tongyoung mine is located about 15 km east of the Samsan Cu mineralized area. These granodiorite stocks in the Samsan and Tongyoung area probably form part of

Table 1. K-Ar and Rb-Sr data of specimens from the Samsan Area.

K-Ar data

Sample description	(%) K	Radiogenic ^{40}Ar (cc/g) (STP$\times 10^{-6}$)	% radiogenic ^{40}Ar	Date (Ma$\pm 1\sigma$)	
Alteration sericite	6.80$\pm$ 0.14	22.09$\pm$ 0.22	2.3	81.84$\pm$ 1.78	this study

Rb-Sr data: two-point isochron

Sample description	$^{86}Sr_{ppm}$	$^{87}Rb_{ppm}$	$^{87}Sr/^{86}Sr$	$^{87}Rb/^{86}Sr$	Isochron parameters slope($\times 10^{-3}$)	intercept	Date (Ma$\pm 1\sigma$)	Reference
Granodiorite								
Whole-rock	52.10	63.94	0.7052	1.210	1.494(6)	0.7034(7)	105.0$\pm$ 5.0	Shelton et al. (1990)
Biotite	3.66	64.89	0.7296	17.540				

the igneous mass. Sericite from an alteration halo adjacent to the quartz vein in the area yielded a K-Ar date of 81.84$\pm$ 1.78 Ma, indicating that mineralization is late Cretaceous, and possibly associated with Cretaceous granodiorite occurring as stocks around the area.

ORE VEINS

The Cu-bearing hydrothermal veins are located in the Cretaceous sedimentary and volcanic rocks of the Yucheon Group (Fig. 1). The veins within the mineralized area fill north-trending fissures and breccia-filled fractures. The breccia zones rarely exceed 2.5 m in width and contain fragments of wall rock up to 30 cm in diameter. Small quartz veins, up to 5 cm wide, fill the spaces between the breccia fragments.

The Jinheung mine was the largest copper producer in the Samsan area. The copper deposit is composed of at least nineteen hydrothermal quartz veins, developed along 4~100 cm wide fractures trending 350° to 010° or 290° to 300° which have total run generally 110 to 400 m with an inclination of 60° to 85°W or E.

The Samsan mine worked three principal quartz veins. The veins generally strike 350° to 010° with dipping 50° to 80°W or 75° to 80°E. The veins are traced about 500 m along the strike direction and vary in thickness from 20~80 cm.

The Daedun mine is composed of the two principal veins with numerous thin subparallel veins. The principal quartz vein is narrow, $\leq$100 cm.

These Cu-bearing hydrothermal veins of all mines (Jinheung, Samsan and Daedun mines) have similar mineralogies and paragenetic sequences, and each includes multiple generations of quartz, with chalcopyrite and sphalerite as the dominant ore minerals.

MINERALOGY AND PARAGENESIS

The mineralogy of all orebodies in the area is simple and is divided into two main paragenetic stages which were terminated by the onset of tectonic activity that is expressed by renewed faulting, brecciation and fracturing. The stages are: stage I, the main stage of ore mineralization, divisible into early substage, during which quartz with amethyst, pyrite and arsenopyrite were deposited, main substage and late substage, which are not separated from early substage by tectonic activity and which are marked by deposition of chalcopyrite and sulfosalt minerals with hematite, respectively; stage II, a stage during which calcite with minor amounts of barite was deposited (Fig. 2). The mineralogy and paragenesis are consistent among the mines in the area.

Stage I

During the stage I, milky and white to clear quartz and amethyst, with economic concentrations of copper, base-metal sulfides and rare sulfosalts were deposited. Stage I mineralization can be classified into three substages based on the mineral assemblages and textural relationships (the fracturing and brecciation of the earlier-deposited vein materials); the early, main, and late substages (Fig. 2).

Early substage of the stage I is characterized by pyrite-arsenopyrite-dark brown sphalerite with milky quartz, amethyst and minor amounts of chlorite and epidote as vein minerals. Pyrite occurs mainly as subhedral fine grains, and rarely as massive band with arsenopyrite (29.0 to 31.4 atomic % As) along vein margins. Dark green chlorite and light green epidote occur as masses or aggregates in the early to main portions of the stage I veins. These are primary hydrothermal minerals.

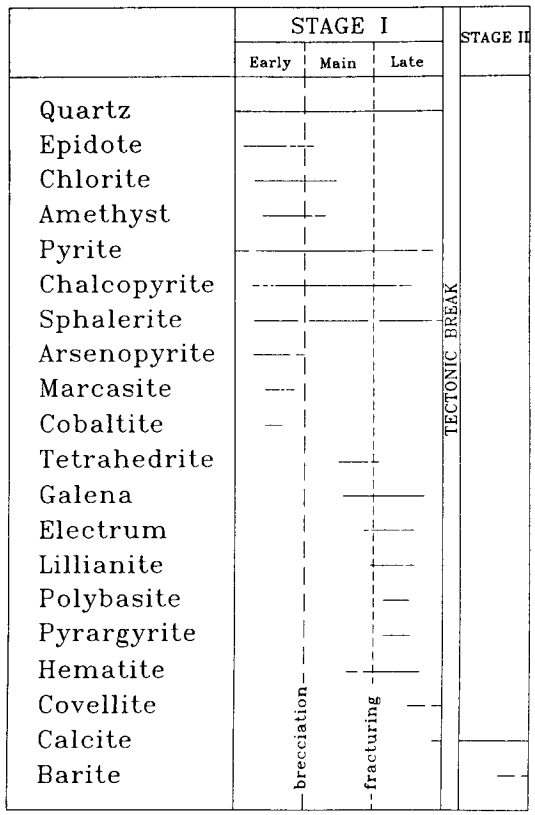

Fig. 2. Generalized paragenetic sequence of vein minerals from Jinheung, Samsan and Daedun Cu veins of the Samsan area.

Minerals of the main substage are characterized by variable proportions of chalcopyrite, sphalerite, and galena with small amounts of tetrahedrite and rare electrum. Chalcopyrite, the most dominant Cu-bearing minerals in the area, is occurred as irregular masses and fine-grained disseminations. Throughout the stage I, chalcopyrite grew together with other sulfides, sulfosalts and/or hematite. Sphalerite is widely distributed throughout the stage II veins: a) the sphalerite of the early substage has relatively high Fe contents (12 to 16 mole % FeS); b) sphalerite with chalcopyrite and/or early galena associated with tetrahedrite as exsolution or intergrowth in main substage (4 to 10 mole % FeS); and c) sphalerite occurs as euhedral masses associated with galena and sulfosalts and with relatively lower Fe contents (1 to 4 mole % FeS, Fig. 3). Some sphalerite with lower FeS contents (<2.0 mole %) is introduced in vugs of stage I veins. Tetrahedrite occurs with chalcopyrite, sphalerite and galena.

The late substage minerals of stage I include ga-

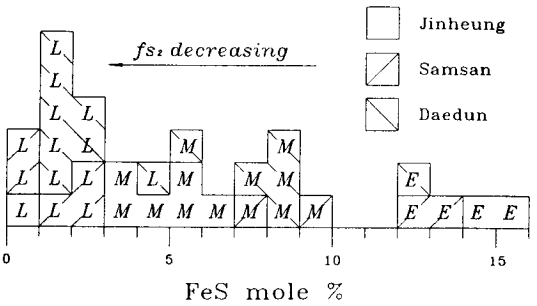

Fig. 3. Variation of FeS content of stage I sphalerite from Jinheung, Samsan and Daedun mines. Capitals in symbols: E, early substage; M, main substage; L, late substage.

lena, sphalerite, sulfosalts and hematite within minor amounts of base metal sulfides. Sulfosalts occur mainly as rounded or irregular grains in galena or sphalerite, and are interstitial to other sulfides or euhedral quartz crystals near vugs. Hematite occurs as euhedral crystals. It is disseminated within the center of the stage I quartz veins. Hematite is commonly interstitial to euhedral quartz crystals near vugs. Hematite is characteristic of all later stage I mineralization, suggesting a distinct change in fluid conditions in later period of the stage I.

Stage II

The last phase of tectonic fracturing created new open-spaces which filled during stage II mineralization. The stage II was not an important ore-forming stage, and it predominantly formed calcite and a minor amount of barite. Minor barite characteristically had overgrown the calcite.

CHLORITE SOLID SOLUTION FOR GEOTHERMOMETRY

Chlorite Occurrences and Compositions

Chlorite is introduced in the hydrothermal veins (stage I veins) and alteration zone in the area. Chlorite in the veins occurs as massive aggregates intergrown within milky quartz, epidote and early stage I sulfides (especially, sphalerite and chalcopyrite). Chlorite also occurs as narrow massive bands near vein margins. These chlorites are often cross-cut by the later ore minerals and other gangue minerals. The chlorite is clearly primary hydrothermal mineral supported by their occurrences. Chlorite in the alteration zone occurs ubiquitous as fine mosaic aggre-

gates with other alteration minerals. Representative compositions (Table 2) show a wide variation of Fe/(Fe+Mg) ratios, varying from 0.49 to 0.83 (chlorite in the vein, 0.49~0.67; chlorite in the alteration zone, 0.49~0.83).

Fig. 4 shows the plots of chlorite analyses on a diagram designed by Hey (1954). These data indicate the wide range of chlorite solid solution in both Si-Al and Mg-Fe. These chlorites are ripidolite, brunsvigite and daphnite.

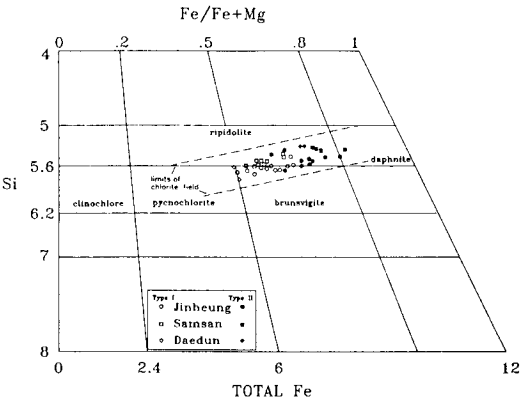

Fig. 4. Hey diagram (Hey, 1954) with plots of analyses outlining a solid solution field of chlorite from the Jinheung, Samsan and Daedun deposits. Type I and type II represent the chlorite occurring in the vein and alteration zone, respectively.

Formation Temperature of Chlorite

Cathelineau and Nieva (1985) have used the Al^{iv} (Al in tetra site) content of chlorite and measured temperatures from deep drill holes in the Los Azufres (Mexico) geothermal field to construct a chlorite solid solution geothermometer. The authors find that Al^{iv} increases with temperature according to the function: $T℃=106\ Al^{iv}+18$ (for 8Si+Al in tetra site, $Al^{iv}_{corrected}=Al^{iv}_{sample}\pm 0.7$ Fe/Fe+Mg). The effect of pressure on the position of the chlorite solid solution field is unknown, but the function which was suggested by Cathelineau and Nieva (1985) came from a maxium depth of p=700 bars. Therefore, the pressure correction should be small for samples used in this study

Table 2. Representative microprobe analyses of chlorite in the vein and alteration zone from Samsan area.

Mine	JINHEUNG								
Type	Type I					Type II			
Sample no.	JH 16-1	JH 30-1	JH 30-2	JH 30-3	JH 30-4	JH 7-1	JH 16-2	JH 16-3	JH 27-1
SiO_2	26.43	24.14	25.48	25.82	26.35	24.57	25.77	24.24	23.57
TiO_2	0.08	0.04	0.00	0.05	0.07	0.12	0.05	0.03	0.06
Al_2O_3	19.74	19.43	19.16	18.77	17.81	19.50	19.04	20.55	19.01
FeO	29.63	30.71	30.89	30.12	25.16	33.66	30.02	29.64	37.24
MnO	1.97	2.51	2.29	1.99	2.27	1.28	1.99	2.64	1.68
MgO	11.12	8.58	9.79	10.55	13.97	7.88	10.44	9.43	5.31
CaO	0.00	0.05	0.02	0.04	0.10	0.00	0.04	0.00	0.00
Na_2O	0.00	0.04	0.04	0.00	0.00	0.01	0.02	0.00	0.00
K_2O	0.05	0.00	0.02	0.00	0.02	0.02	0.01	0.00	0.00
H_2O	11.19	11.00	11.06	11.12	11.35	11.93	11.13	11.09	12.69
Total	100.21	96.50	98.75	98.46	97.10	98.97	98.51	97.62	99.56
Si	5.66	5.48	5.60	5.66	5.72	5.52	5.66	5.38	5.44
Al (iv)	2.34	2.52	2.40	2.34	2.24	2.48	2.34	2.62	2.56
Al (vi)	2.64	2.68	2.58	2.52	2.34	2.68	2.58	2.78	2.62
Mg	3.54	2.90	3.22	3.46	4.54	2.64	3.42	3.12	1.82
Fe	5.30	5.82	5.68	5.52	4.60	6.32	5.50	5.52	7.18
Mn	0.36	0.48	0.42	0.38	0.42	0.24	0.36	0.50	0.32
Ti	0.02	0.00	0.00	0.00	0.02	0.02	0.00	0.00	0.02
Octahedral cations	11.86	11.88	11.90	11.88	11.92	11.90	11.86	11.92	11.96
Fe+Mg	8.84	8.72	8.9	8.98	9.14	8.96	8.92	8.64	9.00
Fe/Fe+Mg	0.60	0.67	0.64	0.61	0.50	0.71	0.62	0.64	0.80
T(℃)[1]	311	335	320	312	293	334	324	343	349

Table 2. Continued.

Mine	SAMSAN						DAEDUN			
Type	Type I			Type II			Type I		Type II	
Sample no.	SS 5-2	SS 6-1	SS 10-1	SS 5-1	SS 5-3	SS 7-5	DD 21-1	DD 22-3	DD 7-1	DD 26-1
SiO_2	25.25	25.76	24.70	23.74	23.46	23.85	25.93	26.68	23.78	23.93
TiO_2	0.06	0.00	0.17	0.00	0.05	0.08	0.00	0.03	0.08	0.04
Al_2O_3	19.91	19.11	20.09	21.62	20.59	20.66	18.27	18.11	20.34	21.43
FeO	30.82	27.23	30.45	32.05	35.29	33.36	25.23	24.47	34.10	30.91
MnO	2.76	0.99	2.34	3.85	3.37	2.16	2.34	2.44	1.87	2.20
MgO	9.66	13.26	9.84	6.49	4.13	7.07	14.99	14.35	7.23	8.90
CaO	0.00	0.07	0.00	0.00	0.00	0.01	0.01	0.02	0.02	0.00
Na_2O	0.00	0.01	0.07	0.00	0.07	0.06	0.00	0.00	0.00	0.00
K_2O	0.07	0.01	0.05	0.00	0.00	0.00	0.00	0.01	0.05	0.00
H_2O	12.05	11.32	11.74	11.89	10.73	11.92	12.40	12.53	11.87	11.95
Total	100.58	97.76	99.45	99.64	97.69	99.17	99.17	98.64	99.34	99.36
Si	5.60	5.46	5.44	5.34	5.38	5.36	5.64	5.82	5.34	5.28
Al (iv)	2.40	2.64	2.56	2.66	2.62	2.64	2.36	2.18	2.66	2.72
Al (vi)	2.50	2.68	2.64	2.92	2.96	2.82	2.32	2.46	2.74	2.86
Mg	4.30	3.24	3.22	2.18	1.42	2.36	4.86	4.66	2.42	2.54
Fe	4.96	5.60	5.60	6.04	6.78	6.26	4.58	4.46	6.40	5.70
Mn	0.18	0.40	0.44	0.74	0.66	0.42	0.24	0.26	0.36	0.42
Ti	0.00	0.00	0.02	0.00	0.00	0.02	0.00	0.00	0.02	0.00
Octahedral cations	11.94	11.92	11.92	11.88	11.82	11.88	12.00	11.84	11.94	11.52
Fe+Mg	9.26	8.84	8.82	8.22	8.20	8.62	9.44	9.12	8.82	8.24
Fe/Fe+Mg	0.54	0.63	0.63	0.73	0.83	0.73	0.49	0.49	0.73	0.69
T(℃)[1]	331	313	336	354	357	352	304	285	354	355

Cation formula based on eight Si+Al(iv) atoms: H_2O calculated from chlorite stoichiometry: Type I and II represent the chlorite in quartz vein and alteration zone, respectively. [1]Formation temperature of chlorite calculated from the equation Cathelineau and Nieva (1985).

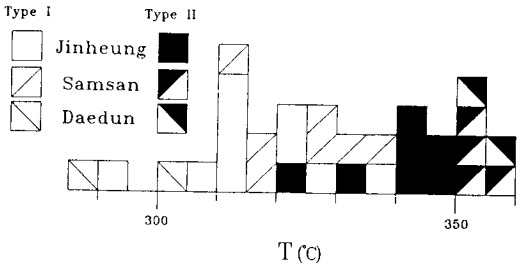

Fig. 5. Frequency diagram of calculated formation temperatures of chlorites from the area. Type I and type II represent the chlorite occurring in the vein and alteration zone, respectively.

(see, Boiling and fluid pressure).

Using the above calibration and adjustments, the chlorites in the Samsan area yield an extrapolated temperature of formation about 285° to 357℃ (Jinheung mine, 293° to 349℃; Samsan mine, 313° to 357℃; Daedun mine, Table 2 and Fig. 5). The calculated formation temperatures of the primary hydrothermal chlorites (285° to 336℃, Fig. 5) are relatively lower than those of the chlorites in alteration zone. The occurrence of chlorite in the vein would be closely associated with early to main copper precipitation.

FLUID INCLUSION STUDIES

Fluid inclusions were examined in 95 samples of stage I and II vein minerals, milky and white to clear quartz, amethyst, sphalerite and calcite in order to document the ranges of fluid compositions and temperatures during the mineralization and to investigate their variations in them. Temperatures of homogenization and ice melting have standard errors of ± 2.0℃ and ± 0.2℃, respectively. Salinity data are based on freezing point depression in the system H_2O-NaCl (Potter et al., 1978). Results of heating and freezing

studies of fluid inclusions are presented in Figures 6 through 8.

Compositional Types of Fluid Inclusions

Two main types of primary and secondary fluid inclusions were observed: liquid-rich and vapor-rich.

Liquid-rich inclusions commonly have 15 to 40 volume percent vapor bubble at room temperature. These inclusions homogenized to the liquid phase upon heating. Vapor-rich inclusions contain a liquid, and vapor bubble comprising about 60 to 90 volume percent at room temperature, and they homogenize to the vapor phase and occur only as primary inclusions in early to main portions of stage I quartz. Both the liquid and vapor-rich inclusions clusters in stage I quartz, homogenized simultaneously to the liquid and vapor phases, respectively. This is generally considered as primary facies evidence for boiling of the hydrothermal fluid at the time of entrapment. The measurements of homogenization temperature for the vapor-rich inclusions were difficult to obtain due to the invisibility of the last remnants of liquid. Bodnar et al. (1985) showed that the data of vapor-rich inclusions should be regarded as the minimum estimates because such a visual estimate may underestimate the true homogenization temperature by up to 300℃. Therefore only a few data with the optimum precision and accuracy were obtained.

A few other inclusions contained three phases; liquid, vapor, and solid. None of the solids resemble NaCl or other salts that could be interpreted as daughter minerals. The solids appear to be captured minerals (Roedder, 1967) or cognate crystal derived from the walls of the inclusions.

The gas bubbles are considered to be primarily H_2O vapor, as there is no clathrate ($CO_2 \cdot 5.75\ H_2O$) during freezing. The absence of CO_2 is also supported by the crushing tests of each type fluid inclusion.

Fluid Inclusion Data

Fluid inclusions in stage I minerals

Minerals examined for fluid inclusions in early substage of stage I were milky quartz and amethyst. They contain numerous liquid-rich and a few vapor-rich primary inclusions. These fluid inclusions homogenize over a range of 245° to 409℃. The main populations of homogenization temperatures for primary inclusions in milky quartz and amethyst from Jinheung mine occur in the ranges of 245° to 409℃ and 251° to 405℃, respectively (Fig. 6). Salinities are in the range of 3.1 to 12.3 equiv. wt. percent NaCl

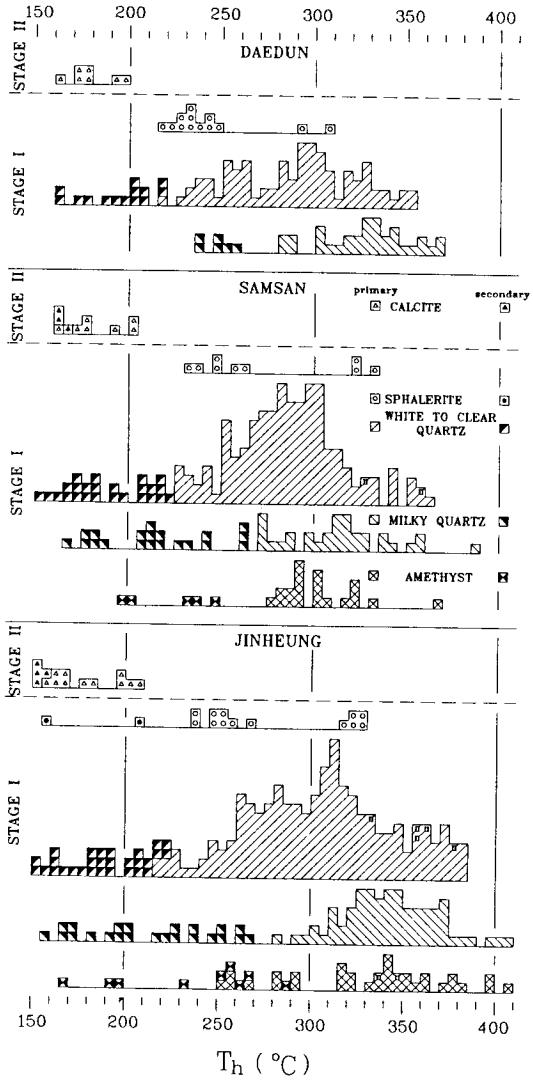

Fig. 6. Frequency diagram of homogenization temperatures of fluid inclusions in vein minerals of the Jinheung, Samsan and Daedun mines. II=two-phase, vapor-rich inclusions.

(Fig. 7). Homogenization of primary inclusions for Samsan mine occurs at temperatures between 263° and 385℃, with a peak temperature of about 310℃ (Fig. 6). Salinities are in the range of 2.2 to 10.8 equiv. wt. percent NaCl (Fig. 7). Homogenization temperatures of primary liquid-rich inclusions in early substage milky quartz of Daedun deposit are relatively lower, 280° to 370℃. Salinities of inclusions in milky quartz range from 5.6 to 9.8 equiv. wt. percent NaCl.

The following are homogenization temperatures for

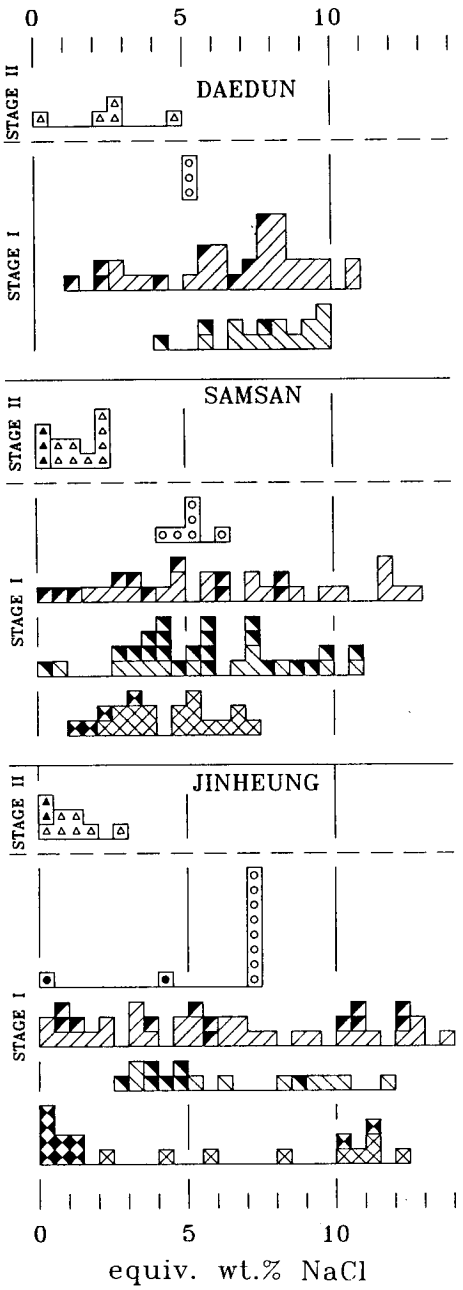

Fig. 7. Frequency diagram of salinities of fluid inclusions in vein minerals of the Jinheung, Samsan and Daedun mines. Symbols are the same as in Fig. 6.

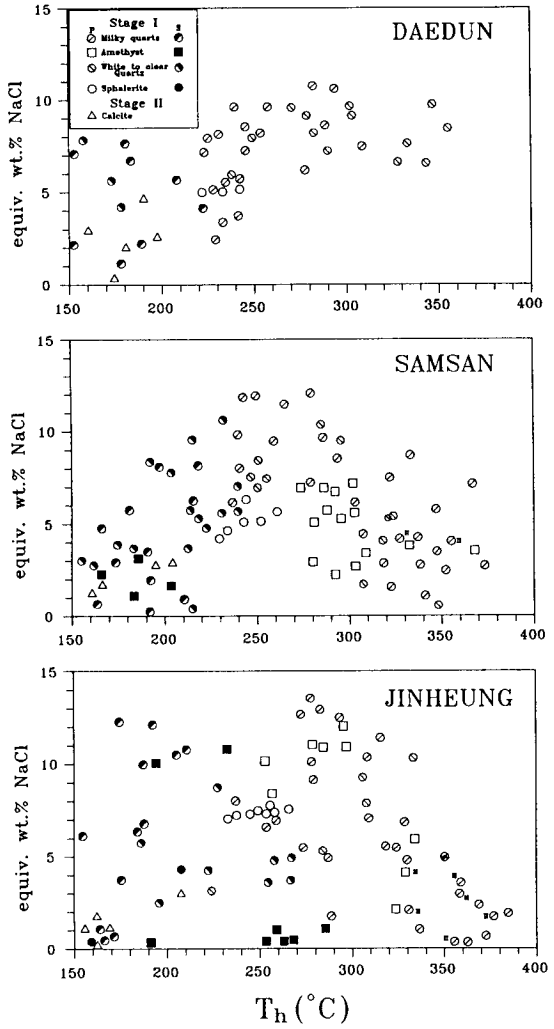

Fig. 8. Homogenization temperature versus salinity diagram for primary and secondary inclusions in stage I and II minerals from the Jinheung, Samsan and Daedun mines. P=primary fluid inclusions, S=secondary fluid inclusions. 'II' beside symbol represents type II, vapor-rich, inclusions.

the primary liquid-rich and vapor-rich inclusions in main and late substage white to clear quartz: Jinheung, 218° to 383℃; Samsan, 225° to 363℃; Daedun, 216° to 353℃ (Fig. 7). Homogenization temperatures of primary liquid-rich fluid inclusion in sphalerite of main substage range from 293° to 334℃. Salinities estimated from primary fluid inclusions in white to clear quartz are 0.3 to 13.9 equiv. wt. percent NaCl (Fig. 7).

Fluid inclusions of late substage yellowish brown sphalerite were studied. Homogenization temperatures have the ranges of 235° to 268℃ (Fig. 6). The measured salinities for the sphalerite are in the range of 4.6 to 7.4 equiv. wt. percent NaCl (Fig. 7).

Fluid inclusions in stage II minerals

Rhombohedral white to clear calcite contains primary and rare secondary liquid-rich inclusions which are ≤20 μm in size. Homogenization temperatures of primary liquid-rich inclusions in calcite range from 156° to 208℃. Salinities estimated from fluid inclusions in calcite are 0.3 to 4.8 equiv. wt. percent NaCl (Fig. 7).

Temperature-Salinity Relationships and Fluid Evolution

Variations in temperature and composition of the evolving hydrothermal fluids during successive mineralization episodes are recorded by fluid inclusions. The relationship between homogenization temperatures and salinities of inclusions in stage I and II vein minerals (Fig. 8) indicates a complex history of boiling, cooling, mixing and dilution.

Some of the vapor-rich fluid inclusions in milky and white to clear quartz of stage I homogenized from ≈320° to 380℃, and they were trapped at the same time as liquid-rich fluid inclusions with the same temperature range. Therefore, during early mineralization, boiling of ore fluids resulted in an inverse relationship between homogenization temperature and salinities. Fluid boiling that deposited the early quartz resulted in an increase in fluid salinity (up to 15 equiv. wt. percent NaCl) at temperatures near 290℃. Simple cooling, and slight dilution by mixing with cooler, less saline fluids, occurred during and after the boiling in the residual fluids. During the main part of stage I, boiling of hydrothermal fluids led to high, but variable salinities. Later cooling and dilution by mixing with cooler, less saline, less-evolved meteoric waters resulted in the positive linear relationship between temperature and salinities shown in Fig. 8. The fluids ranged from a high temperature, high salinity end-member (by boiling) toward a lower temperature, less saline component. By the advent of stage II carbonate deposition, cooling and dilution were more pronounced (temperature, 208° to 156℃; salinity, 0.3 to 4.8 equiv. wt. percent NaCl), probably due to repeated fracturing that allowed more dilute meteoric water into the system. These changes would be very likely to have caused the mineral deposition.

Pressure Considerations

Both liquid-rich and vapor-rich fluid inclusions found as clusters in the same samples of stage I quartz, and tend to homogenize simultaneously to the liquid and vapor phases in the range of 320° to 380° C (Fig. 8). This phenomenon indicates that the early ore fluids (about 6 wt. % NaCl) boiled periodically during stage I mineralization which deposited ore and gangue minerals. With the evidence of boiling and with the temperature and salinity known, the pressure and depth of mineralization can be calculated using the data of Sourirajan and Kennedy (1962) and Haas (1971). The calculated pressures range approximately from 100 to 200 bars for stage I. These pressures correspond to a depth of around 1300 to 3000 m or 370 to 850 m, assuming hydrostatic or lithostatic heads. The nature of vein textures (i.e. massive, euhedral, and vuggy) indicates that the pressure regime was converted from near lithostatic to predominantly hydrostatic loads during the mineralization.

Consequently, the mineralization of the studied deposits occurred at depths of approximately 850 to 1300 m under pressure conditions that fluctuated between lithostatic and hydrostatic regimes.

STABLE ISOTOPE STUDIES

Studies have shown the utility of stable isotopes in elucidating the origin and history of hydrothermal fluids and their ore constituents in vein type deposits (Sheppard and Nielsen, 1971; Rye and Sawkins, 1974; Taylor, 1974; Campbell et al., 1984; Shelton et al., 1988). Oxygen isotope compositions of quartz and calcite, hydrogen isotope compositions of fluid inclusion waters, and the sulfur isotope compositions of sulfide minerals were studied. Standard techniques for extraction and analysis were used, as described by McCrea (1950), Grinenko (1962), Hall and Friedman (1963), and Rye (1966). Isotope data are reported in standard δ notation relative to the Vienna SMOW standard for oxygen and hydrogen, Canyon Diablo Troilite (CDT) standard for sulfur, and the Pee Dee Belemnite (PDB) standard for carbon. The standard error of each analysis is approximately ± 0.1 per mil for oxygen, sulfur, and carbon, and ± 2 per mil for hydrogen (Tables 3 and 4).

Sulfur Isotopes

Analyses of sulfur isotopes were performed on 16 hand-picked sulfide minerals (3 pyrite, 3 chalcopyrite, 7 sphalerite, 3 galena; Table 3) in stage I veins from Jinheung, Samsan and Daedun mines. Pyrite and chalcopyrite in the early substage of stage I have $\delta^{34}S$ values of 6.8 to 9.0‰ and 6.8 to 7.0‰, respecti-

Table 3. Sulfur isotope data for stage I minerals from the Samsan area.

Mine	Sample no.	Mineral	$\delta^{34}S$(‰)	T(℃)[1]	$\delta^{34}S_{H_2S}$(‰)[2]	Comments
Jinheung	JH 5	chalcopyrite	5.4	310	5.6	Vein (M)
	JH 9-1	sphalerite	5.2	280	4.9	Vein (M)
	JH 9-2	galena	3.1	270	5.2	Vein (M)
	JH 21	sphalerite	2.9	250	2.5	Vug (L)
Samsan	SS 2	pyrite	6.8	340	5.7	Vein (E)
	SS 4	chalcopyrite	6.8	340	6.9	Vein (E)
	SS 6-1	sphalerite	6.3	300	6.0	Vein (M)
	SS 6-2	galena	3.2	280	5.3	Vein (M)
	SS 7	sphalerite	5.5	280	5.2	Vein (M)
	SS 23	pyrite	9.0	350	8.0	Vein (E)
Daedun	DD 4	sphalerite	2.7	230	2.3	Vug (L)
	DD 1	galena	1.6	250	3.9	Near vug (L)
	DD 5-1	pyrite	5.5	300	4.3	Vein (M)
	DD 5-2	chalcopyrite	7.0	340	7.1	Vein (E)
	DD 12	sphalerite	4.0	240	3.6	Vein (L)
	DD 23	sphalerite	2.7	230	2.3	Near vug (L)

[1]; Based on fluid inclusion data, temperatures and paragenetic constraints and/or formation temperatures of chlorite.
[2]; Using the isotope fractionation equations in Ohmoto and Rye (1979). Abbreviations: E, early substage; M, main substage; L, late substage.

Table 4. Carbon, oxygen, and hydrogen isotope data for various minerals and inclusion fluids, Samsan area.

Mine	Sample No.	Stage	Mineral	$\delta^{13}C$(‰)	$\delta^{18}O$(‰)	T(℃)[1]	$\delta^{18}O_{water}$(‰)[2]	δD_{water}(‰)
Jinheung	JH 6	I	quartz (M)		7.6	330	1.7	−81
	JH 9	I	quartz (M)		7.3	290	0.1	−83
Samsan	SS 7	I	quartz (E)		6.4	330	0.5	−76
	SS 9	II	calcite	−6.8	6.3	150	−6.3	−86
Daedun	DD 23	I	quartz (M)		3.7	310	−2.8	−82
	DD 24	I	quartz (L)		2.5	260	−5.9	−84

[1]; Based on mean fluid inclusion homogenization temperature for each sample and paragenetic constraints.
[2]; Calculated using the isotope fractionation equations of Matsuhisa et al. (1979); a range of ± 10℃ in the fluid inclusion homogenization temperatures results in a range of ± 0.5‰ in the calculated $\delta^{18}O_{water}$ values at temperatures near 200℃.
Abbreviations: E, early substage; M, main substage; L, late substage.

vely. Sulfides from the main substage have the following $\delta^{34}S$ values: pyrite, 5.5‰; chalcopyrite, 5.4‰; sphalerite, 5.2 to 6.3‰; galena, 3.1 and 3.2‰. The late sphalerite and galena have $\delta^{34}S$ values of 2.7 to 4.0 ‰ and 1.6‰, respectively.

Assuming depositional temperatures of 360° to 230 ℃ for the stage I sulfides based on fluid inclusion data and paragenetic constraints, ranges of possible $\delta^{34}S_{H_2S}$ values of the hydrothermal fluid were calculated (Table 3, using fractionation factors compiled by Ohmoto and Rye, 1979). The range of calculated $\delta^{34}S_{H_2S}$ values are 2.3 to 8.0 per mil: pyrite, 4.3 to 8.0‰; chalcopyrite, 5.6 to 7.1‰; sphalerite, 2.3 to 6.0 ‰; galena, 3.9 to 5.3‰ (Table 3). The $\delta^{34}S_{H_2S}$ values appear to decrease with paragenetic time during the

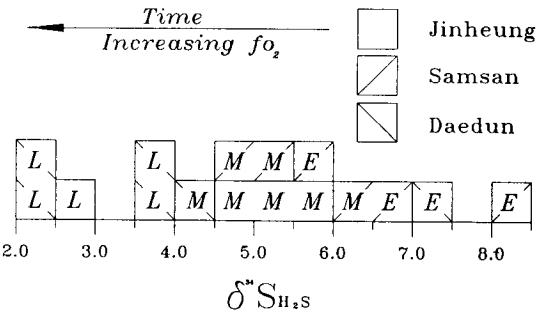

Fig. 9. Sulfur isotope compositions of H_2S in equilibrium with stage I sulfides from the Jinheung, Samsan and Daedun mines. Capitals in symbols: E, early substage; M, main substage; L, late substage.

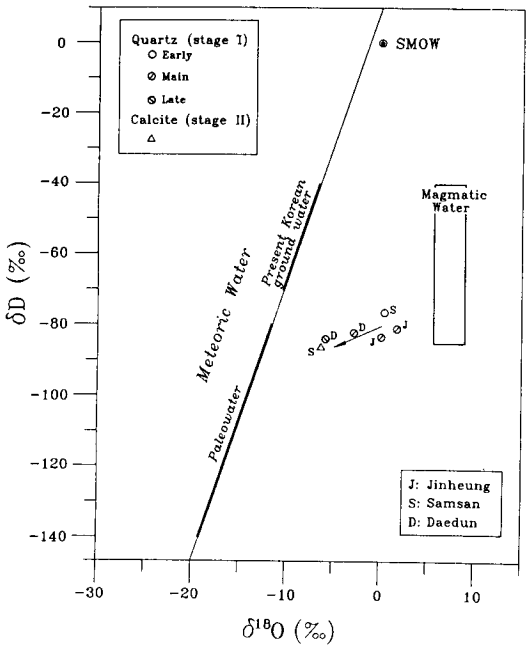

Fig. 10. Hydrogen versus oxygen isotope diagram displaying stable isotope systematics of hydrothermal fluid compositions in the area. The meteoric water line is from Craig (1961); the magmatic water box is from Taylor (1974). Abbreviations: J, Jinheung; S, Samsan; D, Daedun.

stage I from the early substage (5.7 to 8.0‰) through the main substage (4.3 to 6.0‰) to the late substage (2.3 to 3.9‰, Fig. 9).

Oxygen, Hydrogen and Carbon Isotopes

The $\delta^{18}O$ values of five stage I quartz samples from the mines in the area are 2.5 to 8.6‰ (Table 4). Calculated $\delta^{18}O_{water}$ values, using the fractionation equation of Matsuhisa et al. (1979) coupled with fluid inclusion homogenization temperatures, are −5.9 to +1.7‰. Inclusion waters were extracted from the quartz samples. Their δD values are −84 and −76‰ (Table 4). The $\delta^{18}O$ value of one calcite sample from stage II of Samsan deposit is 6.3‰ (Table 4). Using the calcite-water oxygen isotope fractionation equation provided by Matsuhisa et al. (1979) coupled with fluid inclusion homogenization temperature the value of $\delta^{18}O_{H_2O}$ in equilibrium with the calcite was found to be −6.3‰. The $\delta^{13}C$ value of the calcite is −6.8‰ (Table 4). The measured range of δD values of fluids in Cretaceous (142 to 68 Ma) ore-bearing veins in Korea is −80 to −143 per mil (Shelton et al., 1988; So and Shelton, 1987 a, b) and is assumed to represent the range of paleometeoric water compositions in Korea at the time of the mineralization.

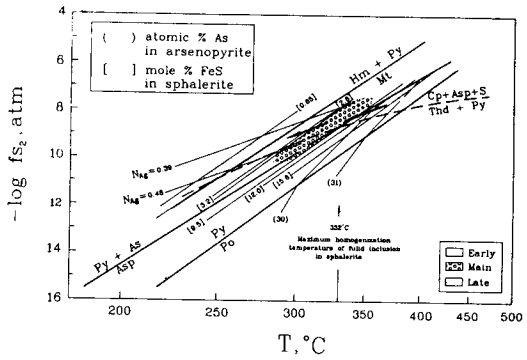

Fig. 11. Temperature versus fugacity of sulfur diagram showing the possible mineralization conditions for early, main and late substage of stage I from the area. Abbreviations: As=native arsenic; Asp=arsenopyrite; Cp=chalcopyrite; Hm=hematite; Mt=magnetite; Po=pyrrhotite; Py=pyrite; S=native sulphur; Thd=tetrahedrite; N_{Ag}= atomic fraction of Ag in electrum.

Fig. 10 shows the distribution of measured and calculated hydrothermal fluid composition from the deposits in the area and the presumed meteoric water at the time of mineralization on a conventional hydrogen versus oxygen isotope diagram. The relationship of calculated $\delta^{18}O_{water}$ values to mineral paragenesis and temperature is a systematic decrease from values of ≈0‰ for early and main substages mineralization of stage I, to −5.9‰ for late substage deposition to −6.3‰ for stage II calcite mineralization. The $\delta^{18}O$ versus δD values of stage I and II minerals plotted in Fig. 10 indicate that a contribution of magmatic water together with meteoric water cannot be ruled out as a source of the fluids that deposited the stage I quartz. The decrease of $\delta^{18}O_{water}$ values with increasing paragenetic time indicates a progressive increase of meteoric water interaction in the Samsan hydrothermal system (Shelton et al., 1987). Quartz from the each substage yielded isotopic values significantly outside the range of those of magmatic water. This could indicate mixing of highly exchanged meteoric water with unexchanged meteoric water, or the exchange of meteoric water with granitic rocks at elevated temperatures and high water/rock ratios. Using either a mixing or exchange model, the isotopic compositions of fluids in the hydrothermal system show a progressive shift from highly exchanged meteoric hydrothermal water dominance in the early and main substage of stage I toward less-or un-exchanged meteoric hydrothermal water dominance in the late substage of stage I and stage II.

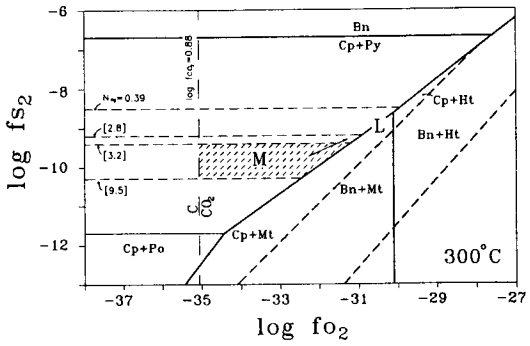

Fig. 12. Plot of log fo_2-fs_2 calculated 300℃ showing mineral stabilities for main and late substages of stage I. Abbreviations: Bn=bornite; Cp=chalcopyrite; Ht=hematite; Mt=magnetite; Po=pyrrhotite; Py=pyrite; N_{Ag}=atomic fraction of Ag in electrum; M=main substage; L=late substage. Numbers in square brackets: FeS content of sphalerite, mole %.

DISCUSSION

Changes in the environmental conditions of the mineralizing fluids during ore mineralization in stage I, the main ore-mineralization stage, veins have been estimated using data from co-existing mineral assemblages, fluid inclusion temperatures, mineral compositions of the arsenopyrite (Fe-As-S; Kretschmar and Scott, 1976), sphalerite (Fe-Zn-S; Scott and Barnes, 1971), and/or electrum (Au-Ag-S; Barton and Toulmin, 1964) and thermodynamic data; these results are summarized in Fig. 11. They will be considered separately for the early substage, the main substage and the late substage (Fig. 11).

Arsenopyrite is associated closely with pyrite in the early mineralization of the early substage and it occurs with early sphalerite having high FeS contents (12.0 to 15.8 mole %) during the mineral deposition of early substage. The As contents of arsenopyrite are from 29.0 to 31.4 atomic percent during the early substage, corresponding to a decrease in log fs_2 values and precipitation temperatures with time from −6.5 to −9.5 atm and from 400° to 320℃ (Fig. 11). The precipitation temperatures are slightly higher (30 ℃) than the fluid inclusion homogenization temperatures in early substage milky quartz and amethyst. These temperature gaps were produced by pressure effects. Early pyrite +sphalerite+chalcopyrite and late chalcopyrite+sphalerite+tetrahedrite+galena assemblages (sphalerite, 3.2−9.5 FeS mole %) in the main substage were precipitated within a temperature range of 280° to 340℃, which corresponds to log fs_2 values of ≈−8.0 to −10.2 (Fig. 11). The late substage mineralization contains more iron-poor sphalerite (2.8 −0.7 mole % FeS), electrum (N_{Ag}=0.39−0.48) and hematite were deposited with galena and sulfosalts. Based on these assemblages and mineral compositions, the precipitation temperatures and log fs_2 values ranged from 240° to 320℃ and ≈−11.2 to −8.5, respecively.

These results indicate that both variables (temperature and fs_2) decreased with paragenetic time. As mentioned previously, the presence of the assemblage hematite+sulfides (and/or sulfosalts) in the later mineralization of the stage II (Fig. 2), as well as the sphalerite compositions, attests to relatively oxidizing fluid conditions. The increasing oxidizing nature of the later stage I fluids may have caused the late substage mineralization. Furthermore, the oxidizing fluid nature may have also led to the stage II barite mineralization. It is further possible to define chemical changes responsible for mineral deposition by using a fugacity of sulfur (fs_2) versus fugacity of oxygen (fo_2) diagram (Fig. 12). The diagram, for convenience, has been constructed for 300℃ in order to compare the main, and late substages of stage I. Actual temperature variations between the two substages (Fig. 6) result in changes in positions of the mineral equilibria but do not affect the overall topology of the diagram.

The occurrence of pyrite and absences of graphite and magnetite in the main substage allow reconstruction of minimum and maximum values of log fo_2 of ≈−35 and ≈−31, respectively. The assemblage magnetite-hematite-pyrite in the late substage indicates a log fo_2 value near −30 (Fig. 12). These results indicate that both variables (temperature and fs_2) decreased and the values fo_2 increased with paragenetic time (especially, from main substage to late substage of stage I). As mentioned previously, there is a decreasing tendency of $\delta^{34}S_{H_2S}$ with time during the stage I mineralization (see, "sulfur isotope"). Two possible explanations for this phenomenon are: 1) gradual addition of sulfur from an isotopically light source, or 2) increase in the SO_4/H_2S ratio of the fluid with time in the equilibrium processes by progressive oxidation of the fluid. From the evidence that follows, we prefer the latter explanations. In either case the original sulfur source must have had a $\delta^{34}S_{\Sigma S}$ value of at least 8.0 per mil. The authors are tempted to interpret that the initial high $\delta^{34}S_{\Sigma S}$ value (8.0‰) represents incorporation of sulfur from an isotopically light source indicating an igneous origin (probably a late Cretaceous granodiorite around the area) and an isotopically heavier source (with $\delta^{34}S$ value >8.0‰, probably the sulfates in surrounding sedimenatry ro-

cks).

In summary, the progressive decreases in temperature and fs_2, apparent concomitant increase in fo_2 and isotopic signatures (sulfur, oxygen and hydrogen isotopes) are interpreted to indicate allowing progressively larger volumes of cooler, more oxidizing meteoric waters during the late substage of stage I and stage II to inundate an early highly exchanged meteoric hydrothermal system.

ACKNOWLEDGEMENTS

This research was financially supported by a grant from the Center for Mineral Resources Research, Korea University.

REFERENCES

Barton, P. B. Jr. and Toulmin, P. III (1964) The electrum tarnish method for the determination of the fugacity of sulfur in laboratory sulfides system. Geochim. et Cosmochim. Acta, v. 28, p. 619-640.

Bodnar, R. J., Burnham, C. W. and Sterner, S.W. (1985) Synthetic fluid inclusions in natural quartz: III. Determination of phase equilibrium properties in the system H_2O-NaCl to 1000℃ and 15000 bars. Geochim. et Cosmochim. Acta, v. 49, p. 1861-1873.

Campbell, A., Rye, D. and Peterson, U. (1984) A hydrogen and oxygen isotope study of the San Cristobal mine, Peru: Implications of the role of water to rock ratio for the genesis of wolframite deposits. Econ. Geol., v. 79, p. 1818-1832.

Cathelineau, M. and Nieva, D. (1985) A chlorite solid solution geothermometer: the Los Azufres (Mexico) geothermal system. Contr. Min. Pet., v. 91, p. 235-244.

Grinenko, V. A. (1962) Preparation of sulfur dioxide for isotopic analysis. Zhurnal Neorganicheskoi Khimii, v. 7, p. 2478-2483.

Hall, W. E. and Friedman, I. (1963) Composition of fluid inclusion, Cave-in-Rock fluorite distirct, Illinois and Upper Mississippi Valley zinc-lead district. Econ. Geol., v. 53, p. 886-911.

Hass, J. L. Jr. (1971) The effect of salinity on the maximum thermal gradient of a hydrothermal system at hydrostatic pressure. Econ. Geol., v. 66, p. 940-946.

Hey, M. H. (1954) A new review of the chlorites. Mineral Mag., v. 30, p. 277-292.

Jin, M. S., Lee, S. M., Lee, J. S. and Kim, S. J. (1982) Lithochemistry of the Cretaceous granitoids with relation to the metallic ore deposits in Southern Korea. J. Geol. Soc. Korea, v. 18, p. 119-131.

Kretschmar, U. and Scott, S. D. (1976) Phase relations involving arsenopyrite in the system Fe-As-S and their application. Canadian Mineralogist, v. 14, p. 364-386.

Lee, M. S. (1981) Geology and metallic mineralization associated with Mesozoic granitic magmatism in South Korea. Mining Geology, v. 31, p. 235-244.

Matsuhisa, Y., Goldsmith, R. and Clayton, R. N. (1979) Oxygen isotope fractionation in the system quartz-albite-anorthite-water. Geochim. et Cosmochim. Acta, v. 43, p. 1131-1140.

McCrea, J. M. (1950) The isotopic chemistry of carbonates and a paleotempreature scale. J. Chem. Physics, v. 18, p. 849-857.

Min, K. D., Kim, O. J., Yun, S., Lee, D. S. and Joo, S. W. (1982) Applicability of plate tectonics to the post-Late Cretaceous igneous activities and mineralization in the southern part of South Korea. Jour. Korean Inst. Mining Geol., v. 15, p. 123-154.

Ohmoto, H. and Rye, R. O. (1979) Isotopes of sulfur and carbon. In: Barnes, H. L. (ed.) Geochemistry of hydrothermal ore deposits. (2nd ed.), John Wiely, New York, p. 509-567.

Park, H. I., Choi, S. W., Chang, H. W. and Lee, M. S. (1983) Genesis of the copper deposits in Goseong district, Gyeongnam area. Jour. Korean Inst. Mining Geol., v. 16, p. 135-147.

Park, H. I., Choi, S. W. Jang, J. W. and Chae, D. H. (1985) Copper mineralization at Haman-Gunbuk mining district. J. Korean Inst. Mining Geol., v. 18, p. 107-124.

Potter, R. W. III, Clynne, M. A. and Brown, D. L. (1978) Freezing point depression of aqueous sodium chloride solutions. Econ. Geol., v. 73, p. 284-285.

Reedman, A. J. and Um, S. H. (1975) The Geology of Korea. Geol. Min. Inst. Korea., 139p.

Roedder, E. (1967) Fluid inclusions as samples of ore fluids. In: Barnes, H. L. (ed.) Geochemistry of hydrothermal ore deposits. Holt Rinehart and Winston, New York, p. 515-574.

Rye, R. O. (1966) The carbon, hydrogen, and oxygen isotopic compositions of the hydrothermal fluids responsible for the lead-zinc deposits at Providencia, Zacatecas, Mexico. Econ. Geol., v. 61, p. 1399-1427.

Rye, R. O. and Sawkins, F. J. (1974) Fluid inclusion and stable isotope studies on the Casapalca Ag-Pb-Zn-Cu deposit, central Andes, Peru. Econ. Geol., v. 69, p. 181-205.

Scott, S. D. and Barnes, H. L. (1971) Sphalerite geothermometry and geobarometry. Econ. Geol., v. 66, p. 653-669.

Shelton, K. L., Taylor, R. P. and So, C. S. (1987) Stable isotope studies of the Daehwa tungsten-molybdenum mine, Republic of Korea: Evidence of progressive meteoric water interaction in a tungsten-bearing hydrothermal system. Econ. Geol., v. 82, p. 471-481.

Shelton, K. L., So, C. S. and Chang, J. S. (1988) Gold-rich mesothermal vein deposits of the Republic of Korea: Geochemical studies of the Jungwon gold area. Econ. Geol., v. 83, p. 1221-1237.

Shelton, K. L., So, C. S., Haeussler, G. T., Lee, K. Y. and Chi, S. J. (1990) Geochemical studies of the Tongyoung gold-silver deposits, Republic of Korea: Evidence of meteoric water dominance in a Te-bearing epithermal system. Econ. Geol., v. 85, p. 1114-1132.

Sheppard, S. M. F. and Nielsen, R. L. (1971) Hydrogen and oxygen isotope ratios in minerals from porphyry

copper deposits. Econ. Geol., v. 66, p. 515-542.
Sillitoe, R. H. (1980) Evidence for porphyry-type mineralization in Southern Korea. Mining Geol., Special Issue, v. 8, p. 205-214.
So, C. S., Chi, S. J. and Shelton, K. L. (1985) Cu-bearing hydrothermal vein deposits in the Gyeongsang Basin, Republic of Korea. Econ. Geol., v. 80, p. 43-56.
So, C. S. and Shelton, K. L. (1987a) Stable isotope and fluid inclusion studies of gold- and silver-bearing hydrothermal vein deposits, Cheonan- Cheongyang-Nonsan mining district, Republic of Korea: Cheonan Area. Econ. Geol., v. 82, p. 987-1000.
So, C. S. and Shelton, K. L. (1987b) Fluid inclusion and stable isotope studies of gold-silver-bearing hydrothermal vein deposits, Yeoju mining district, Republic of Korea. Econ. Geol., v. 82, p. 1309-1318.
Sourirajan, S. and Kennedy, G. C. (1962) The system H_2O-NaCl at elevated temperatures and pressures. Am. J. Sci., v. 260, p. 115-141.
Taylor, H. P. Jr. (1974) The application of oxygen and hydrogen isotope studies to problems of hydrothermal alteration and ore deposition. Econ. Geol., v. 69, p. 843-883.

Manuscript received 14 January 1994

경상분지내 삼산지역 열수동광상에 관한 지화학적 연구

최상훈 · 소칠섭 · 권순학 · 최광준

요 약: 경상분지 백악기 퇴적암류와 화산암류내 열극을 충진한 열수 맥상광체들로 구성된 삼산지역 동광상들은 구조운동에 수반되어 2회에 걸쳐 형성된 석영 및 방해석맥들로 구성된다. 변질대에 산출되는 견운모에 대한 K-Ar 연령은 약 82 Ma로서, 지역주변에 암주상으로 산출되는 화강섬록암의 관입활동 등 후기 백악기 화성활동과 관련된 것임을 지시한다. 주 광화시기인 광화 I기 석영맥내에는 황철석, 유비철석, 황동석, 섬아연석, 방연석, 적철석 및 Pb-Bi-Ag-Sb계 유염광물등의 광석광물들이 녹렴석, 녹니석 등의 맥석광물들과 함께 산출되며, 광화 I기는 광물들의 산출조직과 공생관계 등에 의하여 3개의 substage (early, main, late)로 구분된다. 본역내 광상들에서의 주된 동광화작용은 약 12~3 wt. % NaCl 상당 염농도를 갖는 광화유체로 부터 약 330℃ 에서 약 280℃ 에 걸쳐 진행되었으며, 초기 광화유체의 비등현상으로부터 ≤100~200 bar의 광화작용시 압력이 확인된다. 주광화시기인 광화 I기중 광화유체의 $\delta^{34}S_{H_2S}$값이 초기 8.0‰에서 후기 2.3‰로 점차 감소함은 광화유체의 비등과 천수혼입에 수반되어 산소분압이 점진적으로 증가한 결과로 해석된다. 유체내 산소 및 수소 안정동위원소 연구결과, 이들 동위원소 값이 광화작용의 진행과 함께 점차 감소함은 상대적으로 낮은 water/rock 비값을 갖는 환경하에서 동위원소 교환반응을 이뤄 평형상태에 이른 광화초기 열수계내에 광화작용의 진행과 함께 산화상태의 차갑고 동위원소적 교환반응이 거의 이뤄지지 않은 천수의 혼입이 점증 하였음을 지시한다.